ELSEVIER

Thermochimica Acta 304/305 (1997) 137–150

thermochimica acta

# Photoacoustic and photopyroelectric approach to calorimetric studies

J. Thoen*, C. Glorieux

*Laboratorium voor Akoestiek en Thermische Fysica, Departement Natuurkunde, Katholieke Universiteit Leuven, Celestijnenlaan 200D, B-3001 Leuven, Belgium*

Received 21 July 1996; accepted 29 January 1997

**Abstract**

During the last couple of decades, photoacoustic and photothermal techniques have been used extensively for the study of thermal properties of condensed matter and for thermal wave probing of all kinds of materials and structures. In this paper, we will give a brief account of the basic aspects of the successful standard photoacoustic model with acoustic microphone detection and of a setup with an alternative detection technique with a pyroelectric transducer. The possibilities of these measuring schemes for the simultaneous measurement of the specific heat capacity and thermal conductivity will be illustrated with results from a study of the Curie point of gadolinium and for liquid crystals. © 1997 Elsevier Science B.V.

*Keywords:* Calorimetry; Photoacoustic; Photothermal; Specific heat capacity; Thermal conductivity

## 1. Introduction

The photoacoustic and photothermal effect has been discovered more than a century ago, but gained importance only in the mid-1970s when a proper understanding of the effect in condensed matter was reached. Since that time the field has grown enormously. A multitude of ways of generating the effects has emerged using all kinds of radiation, from laser light to particle beams. Likewise, the diversity in methods for the detection of the generated thermal or acoustical waves has increased dramatically. The international scientific community of scientists working in this field is still vigorously exploring the extensive possibilities of photoacoustic and photothermal methods. One of the reasons for the sudden popularity of this research field is the wide applicability of these techniques and the realized or potential advantages over other techniques. The development of lasers as convenient and powerful localized energy sources has also largely contributed to the success of the field. Applications include trace gas detection, absorption spectroscopy, measurements of static and dynamic thermal quantities, generation of ultrasound, and the nondestructive evaluation of a variety of materials and structures.

In most of the earlier applications in the mid-1970s, details of an optical absorption process were deduced by monitoring the modulated light source heating of a given sample. This type of absorption spectroscopy was named photoacoustic spectroscopy because the heating effect was detected acoustically. Subsequently, a wide range of applications emerged in which an optical source is used as a convenient precisely controlled form of heating. The heating

*Corresponding author.
E-mail: Jan.Thoen@Fys.KULeuven.ac.be.


*PII* S0040-6031(97)00092-0

produced in all cases is nonstationary, resulting in a variety of phenomena associated with the propagation of modulated heat which can be well described in terms of thermal waves. In many applications the detection is nonacoustic and one speaks more appropriately of photothermal phenomena.

In this paper, we will focus our attention on the calorimetric applicability of photoacoustic and photothermal phenomena. The modulated optical source is a common feature in both cases but a substantial diversity may arise from choosing different types of detectors. We will consider two cases, a standard acoustic microphone detection technique and a photopyroelectric detection technique, which during recent years have been successfully used to arrive at high-quality results for the specific heat capacity and thermal conductivity of condensed matter samples.

After a short historical overview we introduce the standard model which was formulated in the 1970s and which contributed tremendously to the growth of the field. Subsequently, we present specific applications for condensed matter. The chosen examples are phase transition studies illustrating the high-resolution possibilities of photoacoustic and photothermal methods.

## 2. Historical background

In 1880, Bell [1] accidentally discovered the photoacoustic effect during experiments with his 'photophone'. At that time, Bell thought that transmitting speech by modulating light waves, as he did in his photophone, was destined to be a better development than his telephone invention. In some way modern fiber optics applications might prove him to be right. He used a beam of sunlight that was modulated by a voice activated mirror attached as a diaphragm to a speaking tube. The light was focused onto a selenium cell in an electrical telephone circuit. The resistance of the selenium was modulated by a modulated light to reproduce speech in the telephone receiver. However, Bell discovered that the selenium (and other solids) attached as diaphragms to hearing tubes emitted audible sound when exposed to intense modulated light.

Within one year, three other papers on photoacoustics were published by Bell [2], Tyndall [3] and Röntgen [4] describing further experiments. It was demonstrated that the effect was not confined to solids but also present in liquids and gases. Bell and his associate S. Tainter [2] convincingly demonstrated that the acoustical signal was in turn dependent on how strongly the incident light was absorbed by the material in the cell. It was also noted from the beginning that the frequency of the sound was the same as the modulation frequency of the light beam.

Several theoretical attempts were formulated to explain this new phenomenon which appeared to be present for all forms of matter, and which was given the name of 'general sonorousness'. These attempts were quite successful for gaseous samples, since in the 1880s the basic gas laws were already well-known. It was correctly assumed that the gaseous sample (in the closed vessel) absorbed all or part of the chopped incident radiation and by doing so increased the kinetic energy of its molecules, thereby giving rise to pressure fluctuations within the cell which were transmitted by the diaphragm of the hearing tube to its own air column and thence to the ear. On the other hand, several attempts were made to account for the phenomenon in condensed matter, but only during the last 15 to 20 years a satisfactory quantitative theoretical understanding has been obtained. The hypotheses of Mercadier [5] and Preece [6] probably came closest to the modern explanation to be given in the next section.

After the initial flurry of interest generated by Bell's original experiments, interest in photoacoustics apparently ceased and no further photoacoustic investigations were performed for almost half a century. An important step forward was achieved in 1938 by Viengerov [7], who employed the photoacoustic phenomenon to study infrared light absorption in gases and to evaluate concentrations of gaseous species in gas mixtures. Substantial improvements were made by Luft [8] pushing the concentration resolution into the ppm region. Modifications of photoacoustic setups could also be used for spectroscopic purposes and were called spectrophones [9]. In addition to straightforward absorption spectroscopy, the photoacoustic effect was also used to study de-excitation and energy-transfer processes in gases [10,11]. During the fifties and the sixties, the photoacoustic effect was primarily used for the study of different aspects of radiationless de-excitation in gases, the gas chromatograph and spectro-photometers being more

versatile. During the last two decades, considerable progress has been achieved by using better radiation sources (e.g. lasers) and improved detection systems (phase sensitive detection and acoustic cells in resonance modes), pushing the detection limits of gaseous species into the ppb region.

In spite of the rebirth of photoacoustics in 1938 and the many years of work with gases since then, photoacoustic studies of solids and liquids remained forgotten until the 1970s, and a satisfactory theoretical explanation was never published. After 1973, however, a strong reemergence of nongaseous photoacoustics occurred. A quantitative theoretical explanation was ultimately obtained and photoacoustics and related photothermal techniques developed into the powerful techniques they are today.

## 3. The standard photoacoustic model

In a typical photoacoustic experiment investigating condensed matter, the sample is placed in a closed cell containing a gas (such as air) and illuminated with modulated (chopped) monochromatic laser light (see Fig. 1). The photoacoustical signal is caused by that fraction of the modulated optical energy which is converted to heat in the sample via nonradiative de-excitation processes. The periodic absorption of light produces a fast decaying thermal wave in the sample but also generates an acoustical wave by the local expansion and contraction of the sample due to the periodic heating. In a general description both types of waves have to be considered [12,13]. There are a broad range of situations where the acoustical wave can be neglected and one only has to consider the thermal wave. The opposite situation can also be realized such as in laser ultrasonics where modulated (or pulsed) lasers are used to generate ultrasonic waves. In a photoacoustic experiment where the thermal wave dominates, by properly choosing the experimental configuration, the one-dimensional model of Rosencwaig and Gersho (RG) [14] can be used for the typical photoacoustic setup of Fig. 1. In the RG model one

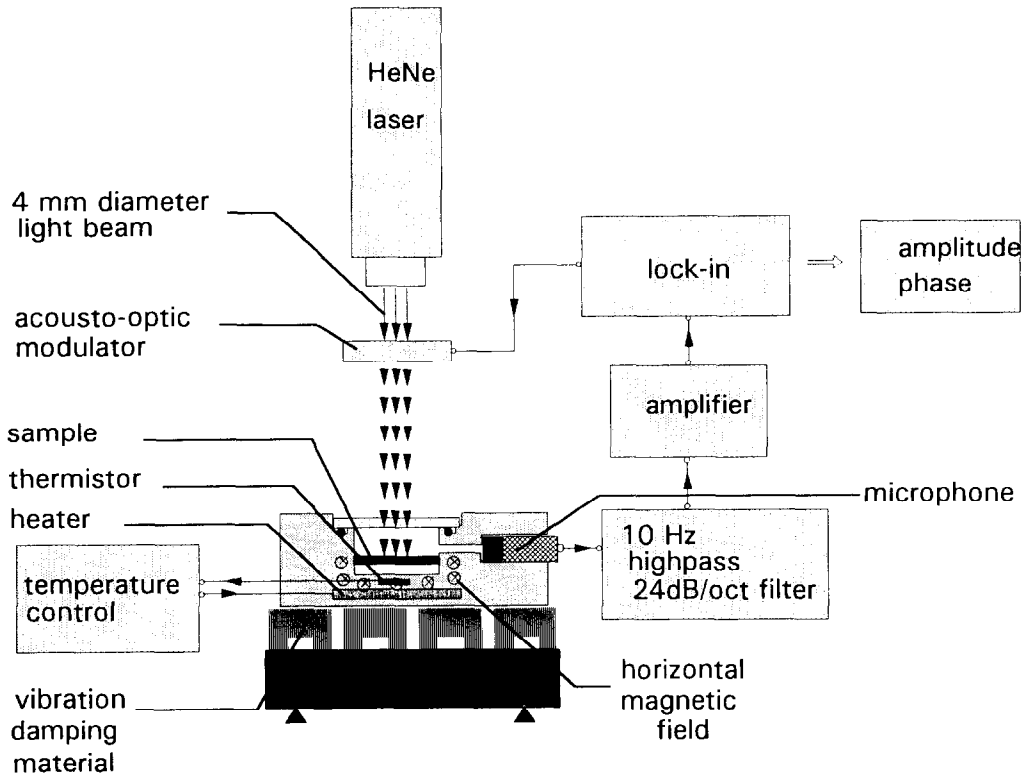


Fig. 1. Schematic representation of a photoacoustic measuring setup.

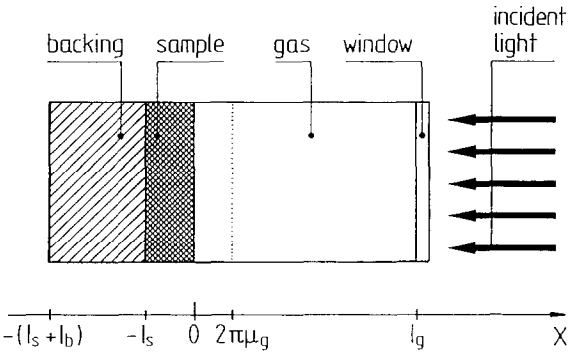


Fig. 2. Schematic cross-sectional view of a simple cylindrical photoacoustic cell, showing coordinates relevant for the standard one-dimensional model.

assumes the incident light intensity to be uniform across the sample, resulting in an amplitude of the thermal source depending only on the depth in the sample and decaying exponentially with the distance from the surface.

In Fig. 2, a schematic cross-sectional view of a photoacoustic cell and the relevant coordinates for the one-dimensional model are given. A microphone detector in contact with the cell gas (through an opening in the cell wall) has been omitted.

In the development of the standard model it is assumed that only the sample absorbs light, thus no heat production occurs in the gas or the backing. For the properties of the gas, sample, and backing we will further use the indices g, s and b, respectively. For harmonically modulated incident monochromatic light, at the wavelength $\lambda$, the following result holds for the heat density produced at any point $x$ in the sample due to light absorbed at that point.

$$H(x) = (1/2)\beta_s(\lambda)I_0(\lambda)(1 + e^{i\omega t})e^{\beta_s(\lambda)x}, \quad (1)$$

where $I_0$ is the light intensity, $\beta_s$ the optical absorption coefficient of the sample and $\omega = 2\pi f$ the angular modulation frequency. In Fig. 2 the $x$-values of Eq. (1) range from $x = 0$ at the gas sample interface to $x = -l_s$ at the sample-backing interface. The gas column extends from $x = 0$ to $x = l_g$ while the backing extends to $x = -(l_s + l_b)$. It is further assumed that $l_g < \lambda_g$ (the wave length of sound at the frequency $f = \omega/2\pi$ in the gas) and that convection (in the gas) and radiation effects are negligible.

A solution for the temperature distribution can be obtained on the basis of the following thermal diffusion equation for the gas, the sample, and the backing:

$$\frac{\partial^2\theta_g}{\partial x^2} = \frac{1}{\alpha_g}\frac{\partial\theta_g}{\partial t} \text{ where } 0 \le x \le l_g, \quad (2)$$

$$\frac{\partial^2\theta_s}{\partial x^2} = \frac{1}{\alpha_s}\frac{\partial\theta_s}{\partial t} - Ae^{\beta x}(1 + e^{i\omega t}) \text{ where } -l_s \le x \le 0, \quad (3)$$

$$\frac{\partial^2\theta_b}{\partial x} = \frac{1}{\alpha_b}\frac{\partial\theta_b}{\partial t} \text{ where } -(l_s + l_b) \le x \le -l_s, \quad (4)$$

where $A = \beta I_0\eta_s/(2\kappa_s)$ and $\theta$ the (complex) temperature. $\alpha = \kappa/\rho C$ is the thermal diffusivity, $\kappa$ the thermal conductivity, $\rho$ the density and $C$ the specific heat capacity. $\eta_s$ is the efficiency at which the absorbed light at wavelength $\lambda$ is converted to heat. Solutions for $\theta$ are obtained assuming continuity of temperature and heat flux at the gas-sample and sample-backing interfaces. Important for the production of the acoustic signal in the gas is the value of $\theta(x, t)$ at the gas-sample interface ($x = 0$), for which Rosencwaig and Gersho [14] arrived at the following expression

$$\theta(0, t) = F_f + \theta_f e^{i\omega t}, \quad (5)$$

where

$$\theta_f = E\left[\frac{(r-1)(b+1)e^{\sigma_s l_s} - (r+1)(b-1)e^{-\sigma_s l_s} + 2(b-r)e^{-\beta_s l_s}}{(g+1)(b+1)e^{\sigma_s l_s} - (g-1)(b-1)e^{-\sigma_s l_s}}\right], \quad (6)$$

where $E = \eta_s\beta_s I_0/[2\kappa_s(\beta_s^2 - \sigma_s^2)]$. In Eq. (5), $F_f$ is the steady-state increase of the temperature at $x = 0$. In Eq. (6), $\sigma_s = (1 + i)a_s$, where $a_s$ is the thermal diffusion coefficient equal to the inverse of the thermal diffusion length of the sample $\mu_s = (2\alpha_s/\omega)^{1/2}$. One further has $r = (1 - i)\beta_s/(2a_s)$, $b = \kappa_b a_b/(\kappa_s a_s)$ and $g = \kappa_g a_g/(\kappa_s a_s)$. The index $f$ refers to the front ($x = 0$) illuminated side of the sample.

In case one has to do with a sufficiently thin sample, that is, the sample thickness $l_s > \mu_s$, there will also be a periodic temperature variation at the sample-backing interface, which we can indicate as a rear thermal signal $\theta_r$. It is possible to arrive at an expression for $\theta_r$ in terms of the sample, backing and gas properties as well. In fact, recently we have reported [15] an extension on the RG model for a $k$-layer system, allowing the derivation of the periodic temperature variation at each interface between layers including the interface between the $(k-1)$th layer and an infinitely thermally thick $k$th layer. Applying that procedure to the situation considered here, we arrive at the following expression for $\theta_r$:

$$\theta_r = E\left[\frac{(g-1)(r-1)e^{-(\beta_s+\sigma_s)l_s} - (g+1)(r+1)e^{-(\beta_s-\sigma_s)l_s} + 2(r+g)}{(g+1)(b+1)e^{\sigma_s l_s} - (g-1)(b-1)e^{-\sigma_s l_s}}\right] \tag{7}$$

Eq. (7) yields the same information as Eq. (6), provided one has a proper temperature sensor at the sample-backing interface.

In standard photoacoustic (PA) microphone detection, the signal is caused by heat transfer at the sample-gas interface to a relatively thin layer of gas ($\simeq 2\pi\mu_g$) adjacent to the front surface of the sample. For the temperature distribution of the periodic component one can derive:

$$\theta_{a.c.}(x,t) = \theta_0(0,t)e^{-\sigma_g x}e^{i\omega t}, \tag{8}$$

with $\sigma_g = (1+i)/\mu_g$. This means that the signal is, indeed, reduced to less than 0.5% at a distance of one wavelength ($= 2\pi\mu_s$) from the sample surface. This boundary layer of gas can then be considered as a thermal piston creating the acoustical signal detected by the microphone in the cell wall. The precise variation, $\delta P_f$, in the gas is obtained by assuming an adiabatic response to this piston [14,16], resulting in:

$$\delta P_f = Q_f \exp(i\omega t - i\pi/4), \tag{9}$$

where

$$Q_f = \frac{\gamma_g P_0 \theta_f}{(2)^{1/2} T_0 l_g a_g} = q_f e^{-i\psi f}, \tag{10}$$

where $P_0$ and $T_0$ are the cell pressure and temperature, respectively and $\gamma_g$ the ratio of the specific heats at constant pressure and constant volume of the gas.

In principle it is possible to arrive, on the basis of Eqs. (6)–(10) at the thermal parameters of a given sample. This, however, demands sufficient knowledge of thermal parameters of both the gas and the backing, as well as of optical parameters ($\eta_s$ and $\beta_s$) of the sample or of the applied coating. Moreover, the relationship between the measured microphone signal and the PA signal can be rather complicated: the photoacoustic cell; the microphone; the amplifiers; and filters do not have a flat frequency response. Therefore, one needs a calibration procedure. This calibration is possible using a reference material with known thermal and optical properties. The measured (superscript m) amplitude $A$ and phase $\psi$ of the sample and reference signal can be written as:

$$A^m_{sample} = A_{sample} \times f_{sys}, \tag{11}$$

$$\psi^m_{sample} = \psi_{sample} \times \psi_{sys}, \tag{12}$$

$$A^m_{ref} = A_{ref} \times f_{sys}, \tag{13}$$

$$\psi^m_{ref} = \psi_{ref} \times \psi_{sys}. \tag{14}$$

The latter two equations yield the system response ($f_{sys}$, $\psi_{sys}$), which can be used to solve $A_{sample}$ and $\psi_{sample}$ in the former two equations. The rather complex expression (6) for the front thermal signal appearing in Eq. (10) for the photoacoustic signal can be substantially simplified by choosing (for examples see further) proper measuring configurations. This possibility results from the fact that in photoacoustic and photothermal experiments one disposes of three length scales which in many cases can be optimally chosen to arrive at the desired thermal (or sometimes optical) information. These length scales are: the sample thickness $l_s$, the optical penetration depth $\beta_s^{-1}(\lambda)$ at a given wavelength $\lambda$ and the thermal diffusion length $\mu_s = (2\kappa_s/\rho_s C_s \omega)^{1/2}$. For a given sample, $\beta_s^{-1}(\lambda)$ can be controlled by changing $\lambda$ and $\mu_s$ by adjusting the modulation frequency $\omega$.

### 3.1. The photopyroelectric detection technique

As already pointed out, one may also choose to detect the rear temperature variation $\theta_r$ of a sample

with a thickness comparable or smaller than the thermal diffusion length. Very attractive setups have been realized for solid as well as for liquid samples by using a pyroelectric sensor as the detector for the a.c. part of the signal.

If one considers a pyroelectric transducer (e.g. a $LiTaO_3$ crystal), with thickness $l_p$ and surface area $A$, in a one-dimensional configuration, a change in the temperature distribution $\theta(x, t)$ relative to an initial reference situation $\theta(x, t_0)$ will cause a change of polarization, this in turn induces an electric charge given by:

$$q(t) = \frac{pA}{l_p}\int_0^{l_p}[\theta(x,t) - \theta(x,t_0)] = \frac{pA}{l_p}\theta_p(t), \tag{15}$$

where $p$ is the pyroelectric coefficient of the transducer. Consequently, a current is produced:

$$i_p = \frac{pA}{l_p}\frac{d\theta_p(t)}{dt}. \tag{16}$$

Normally, the electrical signal from the pyroelectric transducer is detected by a lock-in amplifier. Thus, only the a.c. variation of the temperature is considered. The pyroelectric element can be represented by an ideal current source with a leakage resistance and capacitance in parallel, while the detection electronics can be described by an input capacitance and a parallel load resistance [17]. Circuit analysis [18,19] results in a general expression for the signal $V(\omega)$, which can be written in the following way:

$$V(\omega) = |V(\omega)|e^{i\varphi(\omega)}, \tag{17}$$

where

$$|V(\omega)| = \frac{RpA\omega}{(1+\omega^2\tau^2)^{1/2}}|\theta_p(\omega)|, \tag{18}$$

and

$$\varphi(\omega) = \tan^{-1}(-\omega\tau) + \frac{\pi}{2} + \varphi_p(\omega). \tag{19}$$

In Eq. (18) the time constant $\tau = RC$, with $R$ and $C$ the parallel combinations of the resistance and capacitance of the pyroelectric transducer and detection circuit. $|\theta_p(\omega)|$ and $\varphi_p(\omega)$ are the amplitude and phase of the complex average temperature $\theta_p(\omega)$ over the pyroelectric transducer.

In general Eqs. (18) and (19) can be quite complicated. However, under properly chosen experimental conditions, it is possible to arrive at substantially simplified equations which allow for a simultaneous determination of the specific heat capacity and thermal conductivity of a sample in thermal contact with a pyroelectric transducer. A typical setup [20,21] which can be used for liquid crystals and other fluids is given in Fig. 3. The wavelength of the modulated light, the modulation frequency, and the sample and transducer thickness $l_s$ and $l_p$ are chosen in such a way that the sample and transducer are optically opaque, the detector thermally very thick ($\mu_s \ll l_p$), and the sample quasi-thermally thick ($\mu_s \leq l_s$). In the setup of Fig. 3 the opacity of the sample is realized by means of a thin layer of gold at the interface of the (liquid) sample and a transparent quartz piece. Under these circumstances one obtains for the signal amplitude and phase [22]:

$$|V(\omega)| = \frac{I_0\eta_s ARPe_p}{l_p[1+(\omega\tau)^2]^{1/2}p_pC_p} \times \frac{\exp[-(\omega/2\alpha_s)^{1/2}l_s]}{e_s(e_m/e_s+1)(e_p/e_s+1)}, \tag{20}$$

$$\varphi(\omega) = \tan^{-1}(-\omega\tau) - (\omega/2\alpha_s)^{1/2}l_s, \tag{21}$$

where subscripts s, p, and m, respectively, refer to the sample, the pyroelectric transducer and to the medium in contact with the sample front surface (quartz in Fig. 3). The quantity $e = (\rho C\kappa)^{1/2}$ is the thermal effusivity. From Eq. (21) it is possible to determine the sample thermal diffusivity $\alpha_s$. Inserting $\alpha_s$ in Eq. (20) yields the sample thermal effusivity $e_s$. The specific heat capacity and thermal conductivity of the sample are given by:

$$C_s = e_s\rho_s^{-1}\alpha_s^{-1/2}, \tag{22}$$

and

$$\kappa_s = e_s\alpha_s^{-1/2}. \tag{23}$$

At this point it is worthwhile to make a connection between the above techniques and a.c. calorimetry. In a standard a.c. calorimetric setup [23] the local

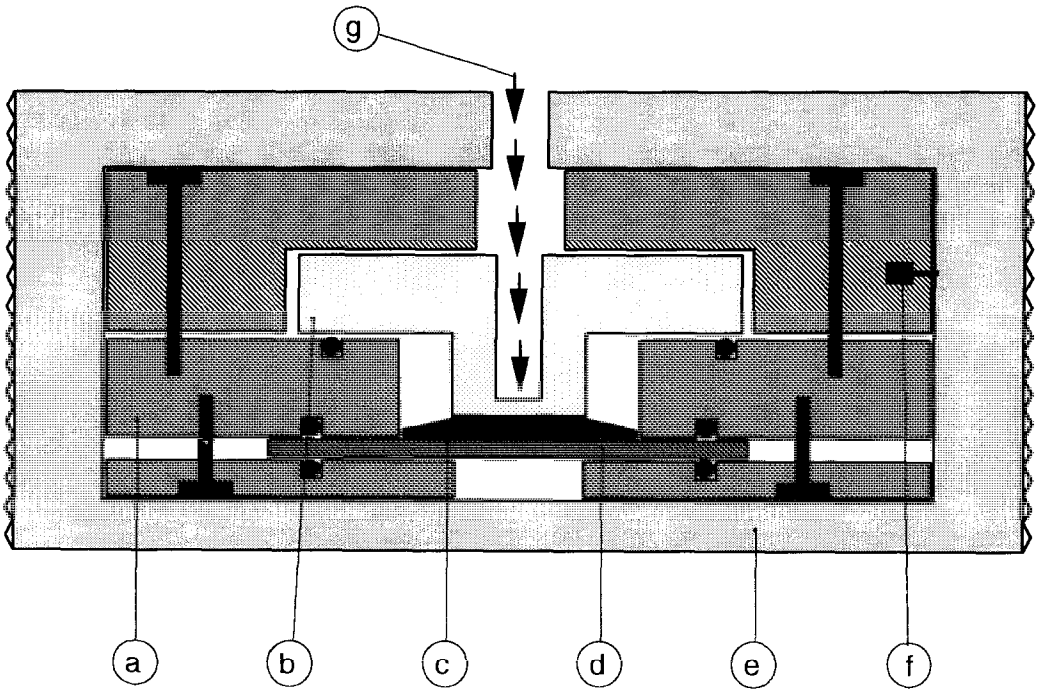


Fig. 3. Schematic representation of a photopyroelectric measuring cell. a: stainless steel holder, b: quartz piece with gold layer in contact with the sample, c: (liquid) sample, d: pyroelectric transducer, e: temperature controlled cell with heating wires on the outside surface, f: thermistor for temperature measurement and control, and g: modulated laser beam.

heat source on one side of the sample (the gold layer in Fig. 3) is normally realized by means of a thin electric current carrying resistance wire; However, optical heating of the sample in a.c. calorimetry has been used as well [24–26]. On the opposite site of the sample detection is made with a small thermistor or a thermocouple in good thermal contact with the sample [23–25] or at least within a thermal diffusion length of the surrounding gas [26]. The main difference between a.c. calorimetry and photoacoustic or photothermal measuring techniques is the range chosen for the measuring frequency. In a.c. calorimetry $\omega$ is chosen such that the sample as a whole experiences the imposed modulation. Thus the sample is considered to be thermally very thin in the sense that the wavelength of the thermal wave is much larger than the sample thickness, that is, $l_s \ll 2\pi\mu_s$. Since no temperature gradient is present in the sample, only the specific heat capacity can be measured.

## 4. Applications

In this section, we would like to illustrate the possibilities of the photoacoustic and photopyroelectric methods by presenting some of our recent results for two different kind of systems. The first one is a photoacoustic investigation of the Curie point of gadolinium and the second one is concerned with the specific heat capacity and thermal conductivity anisotropy of oriented liquid crystals. Indeed, one of the assets of these methods is the fact that in a single experiment one simultaneously can measure the specific heat capacity as well as the thermal conductivity.

### *4.1. The Curie point of gadolinium*

From the point of view of phase transition studies gadolinium is very attractive because it undergoes a second-order ferromagnetic-to-paramagnetic phase transition at room temperature. Its critical behavior

is, however, complicated and not yet fully understood. The ferromagnetic character of gadolinium is believed to be mainly caused by isotropic spin–spin interactions, but there is also an anisotropic hexagonal crystal symmetry present. As a result, close to the critical point one expects a rather complex critical behavior with a pattern of crossover behavior. This makes gadolinium a challenging case for theoretical studies as well as for high-resolution experimental studies.

Although the thermal behavior of gadolinium has attracted a good deal of attention in the past, many aspects could still be much better characterized. This situation encouraged us a few years ago to undertake a high-resolution photoacoustic investigation of the specific heat capacity and thermal conductivity near the Curie point as a function of temperature and magnetic field for three samples of different quality [27]. One of these samples was the high-quality single crystal also studied in detail by Bednarz, Geldart and White [28] by means of a.c. calorimetry (in zero external magnetic field). This, among other things, allowed a comparison between the specific heat capacity determined from a.c. calorimetry with that determined from photoacoustic measurements. In what follows, we will focus on the experimental methodology rather than on the physical interpretation of the results, the latter of which can be found in Ref. [27] and in Ref. [29] where a magnetocalorically generated acoustic signal was used to obtain information on magnetic as well as on thermal parameters of gadolinium samples.

We have used the photoacoustic setup of Fig. 1 to determine simultaneously the temperature and magnetic field dependence of the specific heat capacity and thermal conductivity of gadolinium in the neighborhood of the Curie point. Indeed, choosing a proper photoacoustic measuring configuration allows the simultaneous measurement of $C$ and $\kappa$. In our photoacoustic cell the sample, which is in contact with air on the top and bottom sides, was illuminated by a periodically intensity modulated 10 mW He–Ne beam ($\lambda = 633$ nm). At the chosen wavelength the sample is optically very opaque and Eq. (6) for the front signal reduces to [30]:

$$\theta_f(\omega) = \frac{(1-R)I_0}{2\sqrt{\pi f}} \frac{\exp(\sigma_s l_s) + \exp(-\sigma_s l_s)}{\exp(\sigma_s l_s) - \exp(-\sigma_s l_s)}, \tag{24}$$

with $R$ the sample reflectivity. The modulation was done with an Intraaction type AOM40 acousto-optic modulator. The signal was detected by a Brüel and Kjaer type 4165 microphone followed by a type 2607 amplifier and a PAR 5210 lock-in detector and, after calibration (with a carbon coated sample) converted to surface temperature amplitude and phase information making use of Eq. (24). Since the calibration procedure only allowed for the determination of relative changes in the measured quantities, we have made use of reference data for $C$ and $\kappa$ of gadolinium at 40°C to scale the curves of the thermal properties [27].

The temperature of the photoacoustic cell was automatically controlled with an accuracy better than 0.01 K and was varied with a rate of 0.02 K/min during temperature scans. The magnitude of a magnetic field, oriented parallel to the sample surface (see Fig. 1), was measured by a Hall probe, and controlled by automatically positioning permanent magnets around the photoacoustic cell. The beam width of 4 mm was large enough to fulfill the conditions of one-dimensional heat transport which were assumed in the derivations of the standard model and to arrive at Eq. (24).

A necessary condition for the experimental investigation of phase transitions is that measurement induced thermal gradients are minimal. In our setup, the maximum temperature oscillation (at 800 $Wm^{-2}$ light intensity and at a modulation frequency of 10 Hz) was not more than 13 mK, which is very similar to values used in a.c. calorimetry. The static gradient over the sample (see Eq. (5)) was estimated to be smaller than 20 mK.

In cases where one does not expect frequency dependence of thermal parameters (which is the case here for gadolinium) photoacoustics allows for a simple consistency check of the theoretical model by using different modulation frequencies. Fig. 4 shows that the curves for the thermal diffusivity and thermal effusivity, obtained at 10, 15, 60, 120, and 240 Hz (from a thermally thin to a thermally thick regime) are overlapping within the experimental uncertainty, confirming the validity of Eq. (24) for our experimental configuration. From the effusivity and thermal diffusivity data it is possible to arrive at the specific heat capacity and the thermal conductivity using Eqs. (22) and (23). As an illustration we give in Figs. 5 and 6, $C$ and $\kappa$ results as a function of

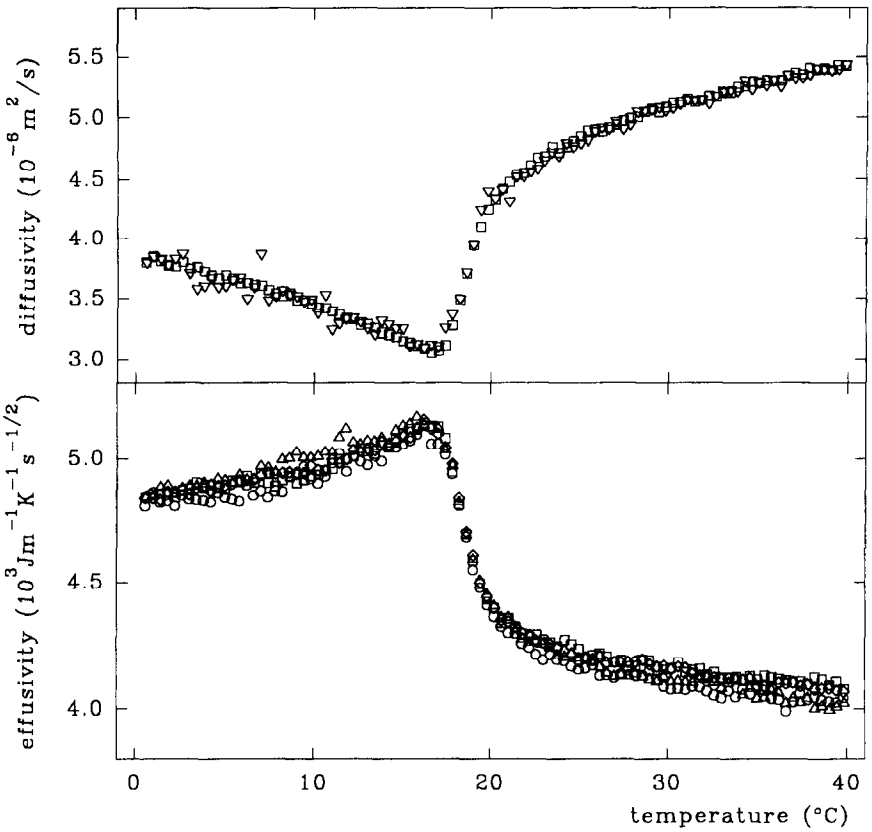


Fig. 4. Thermal diffusivity and effusivity results for a gadolinium sample as obtained from photoacoustic measurements at different modulation frequencies. Circles: 10 Hz, inverted open triangles: 15 Hz, open squares: 120 Hz, and open triangles: 240 Hz.

temperature for three different samples. The results near $T_c$ are strongly dependent on the quality of the sample. Sample 1 was a small ($0.25 \times 5 \times 9$ mm$^3$) piece of 99.9% pure polycrystalline gadolinium. Sample 2 was 365 μm thick 8 mm diameter single crystal disc (purity 99.99%) of commercial quality. Sample 3 is the same high-purity single crystalline Sample II studied by Bednarz, Geldart and White [28] by means of a.c. calorimetry. A comparison between these a.c. results for $C$ and our photoacoustic values for Sample 3 is made in Fig. 7. A very good agreement can be observed. The small systematic deviations at high temperatures are the result of a small error in the slope of the calibration curve. From these results it should be clear that the photoacoustic technique allows one to obtain high-resolution results of the specific heat capacity of quality comparable to those obtained with a.c. calorimetry. Moreover, one obtains simultaneous information on the thermal conductivity as well. It should also be pointed out that, similarly to a.c. calorimetry, one can use rather small samples. Further details on the analysis of these data and other data measured in the presence of external magnetic fields can be found elsewhere [26,29].

### 4.2. *Liquid crystals*

The measurements of thermal quantities have been an important approach for characterizing liquid crystals. High-resolution calorimetric measurements of the static quantities have been extensively carried out using steady-state adiabatic or a.c. calorimetric techniques [31–34]. Thermal transport properties, such as thermal conductivity, have been studied in a limited number of cases using low-resolution steady-state gradient or transient techniques [35]. Recently,

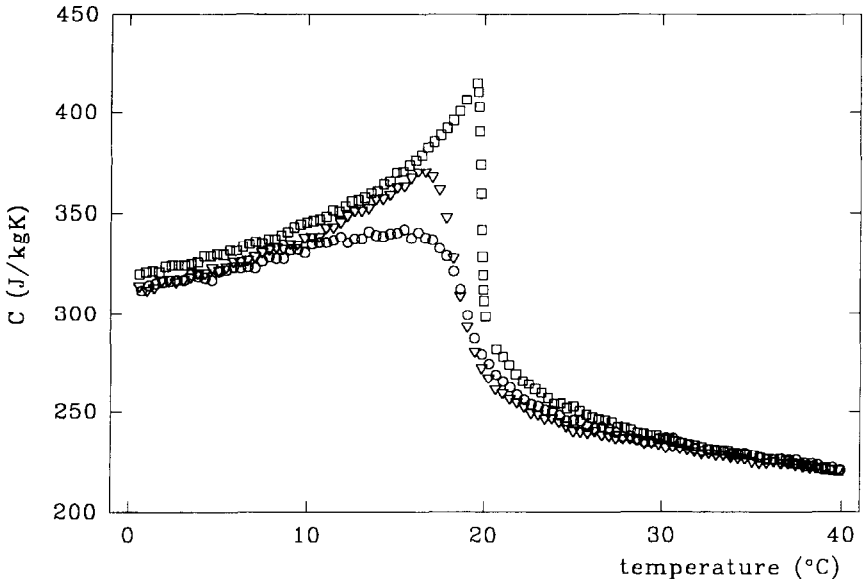


Fig. 5. Photoacoustically determined results for the specific heat capacity near the Curie point of three gadolinium samples of different quality. Sample 1: circles, Sample 2: triangles, and Sample 3: squares.

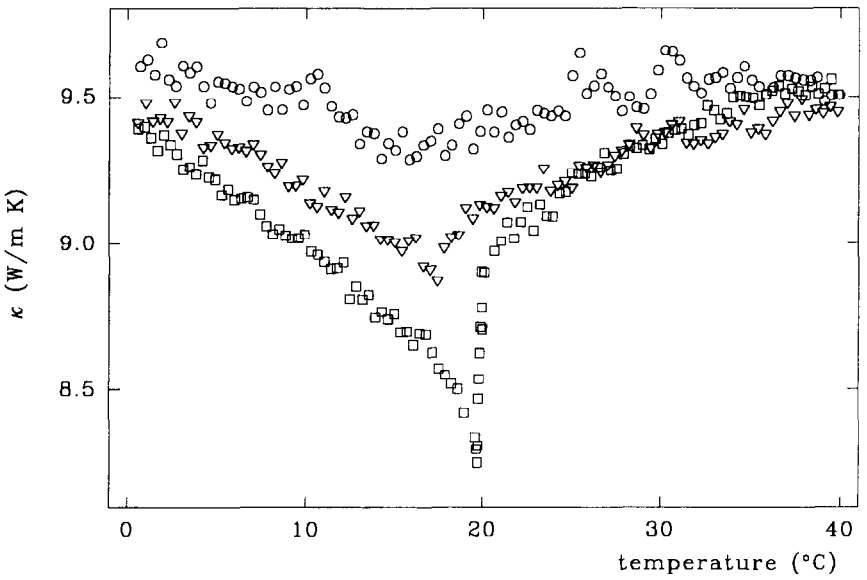


Fig. 6. Photoacoustically determined results for the thermal conductivity near the Curie point of three gadolinium samples of different quality. Sample 1: circles, Sample 2: triangles, and Sample 3: squares.

photoacoustic and photothermal techniques have proven to be capable of high-resolution measurements of the temperature dependence of several static and dynamic parameters in liquid crystals, especially across the region of phase transitions [22,36–40]. An important advantage of these techniques is the fact that they allow for the simultaneous determination of the heat capacity $C$ and the thermal conductivity $\kappa$

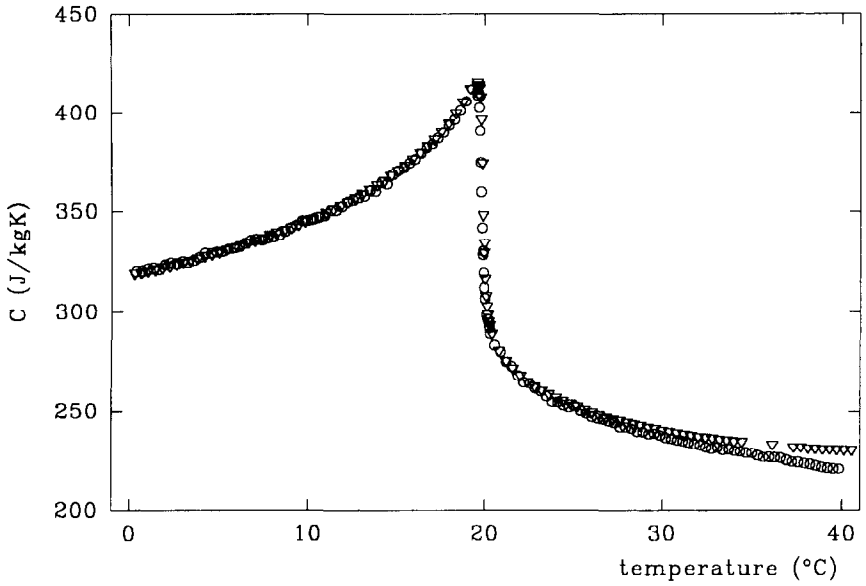


Fig. 7. Comparison of the temperature dependence of the specific heat capacity of a high-quality single crystal gadolinium sample (Sample 3) determined photoacoustically (circles) and from ac calorimetry (triangles) by Bednarz, Geldart and White (Ref. [28]).

for very small liquid crystal samples, given a properly chosen measuring configuration.

For photoacoustic measurements in liquid crystals, one usually works in the optically and thermally thick regime ($e^{\sigma_s l_s} \gg e^{-\sigma_s l_s}$, $e^{-\beta_s l_s}$), resulting in substantially simplified expressions. This means that $\beta_s^{-1}$ and $\mu_s$ of the sample have to be much smaller than the sample thickness $l_s$. The contribution of the backing material then disappears from the expressions. One then obtains for the amplitude $q_f$ and the phase $\psi_f$ in Eq. (10)[36]:

$$q_f = \frac{\gamma_g P_0 I_0 t(2t^2 + 2t + 1)^{-1/2}}{2\sqrt{2} T_0 l_g (1 + s)\kappa_g a_g^2}, \tag{25}$$

and

$$t g\psi_f = 1 + 1/t, \tag{26}$$

where $t = \mu_s\beta_s/2$ and $s = a_s\kappa_s(\kappa_g a_g)^{-1}$. The Eq. (25) and Eq. (26) allow for the simultaneous determination of the specific heat capacity per unit volume ($\rho_s$ $C_s$) and the thermal conductivity $\kappa_s$ of the sample by solving for $t$ and $s$. This gives:

$$\rho_s C_s = \beta_s \kappa_g a_g s t^{-1} \omega, \tag{27}$$

$$\kappa_s = 2\kappa_g a_g s t \beta_s^{-1}. \tag{28}$$

However, one should arrange the measuring condition in such a way that $1/t = 2/(\mu_s\beta_s)$ is not too small compared to 1 in Eq. (26). This can be achieved by a proper choice of the modulation frequency and by controlling the $\beta_s$ value by choosing an appropriate wavelength for the modulated light. Since Eqs. (25)–(28) depend on the value of $\beta_s(\lambda)$, one has to measure this quantity in a separate experiment [20,21]. The other parameters related to characteristics of the cell, the cell gas and the light source are, as already pointed out above, usually taken care of by simultaneous or separate calibration runs with a sample of known optical and thermal parameters [38,39].

During the last 6 to 7 years we have carried out photoacoustic investigations of several kinds of liquid crystals in oriented or partly oriented samples in a photoacoustic cell similar to the one schematically given in Fig. 1. One of the main purposes of these efforts was, in addition to measuring the specific heat capacity anomalies near phase transitions, the investigation of the anisotropy in the thermal conductivity in the liquid crystalline phases. Indeed, the transport of heat along the orientational director (orientation of the long molecular axes) is substantially larger than perpendicular to it. In order to orient the liquid crystals in the proper direction with respect to the heat flow

(imposed by the direction of the modulated laser beam), we used magnetic fields parallel or perpendicular to the free surface of the liquid crystal sample. From our investigations we found out that for many types of liquid crystals a free surface is a strong ordering field, in the sense that it imposes strong homeotropic alignment [38,21]. Even rather strong fields parallel to the sample surface could not break the perpendicular homeotropic orientation of the molecules near the free surface, and resulted in a gradual rotation of the orientational director from perpendicular at the surface to parallel in the bulk of the sample [38,41]. On the other hand, magnetic fields perpendicular to the free surface enhance, also in the bulk, the homeotropic orientation throughout the whole sample and allowed proper measurement of $\kappa_s$ for heat flux parallel to the director. In Fig. 8 results [40] are given for the liquid crystal 8CB (octylcyanobiphenyl) which has a smectic A and a nematic phase below the isotropic phase (above 41°C). The low temperature smectic A-to-nematic phase transition and the nematic-to-isotropic phase transition at a higher temperature are clearly marked by anomalies in the specific heat capacity which are consistent with previously obtained results by means of adiabatic scanning calorimetry [42]. In 1990, Zammit et al. [39] published high-resolution results for the nematic-to-smectic A phase transition in 9CB, 8CB and a mixture of 8CB+7CB (all compounds of the alkylcyanobiphenyl homologous series). The results showed a critical anomaly both in $C_s$ and $\kappa_s$. The results for 9CB were subsequently also confirmed by measurements in a photopyroelectric setup [22]. In both these investigations no effort was made to align the sample. The values of the specific heat capacity critical exponents are fully consistent with previous results obtained by Thoen et al. [42] by means of adiabatic scanning calorimetry. In addition, the thermal conductivity critical exponent values have been obtained, but no agreement with theory or systematic trend could be obtained [39]. It should also be noted that in our oriented sample of 8CB we did not observe a critical effect in $\kappa_s$ at the nematic-to-smectic transition (see Fig. 8). Recent photopyroelectric measurements near the same transition of a nonoriented sample of $\bar{8}S5$ (octyloxythiolbenzoate), also did not show a critical $\kappa_s$ anomaly [43]. New measurements by Scudieri et al. [44] on oriented 8CB samples are consistent with our previously reported $\kappa_s$ results. Whether the previously reported $\kappa_s$ anomaly is an artifact caused by using unaligned samples or by excessive temperature gradients [43], is not entirely clear.

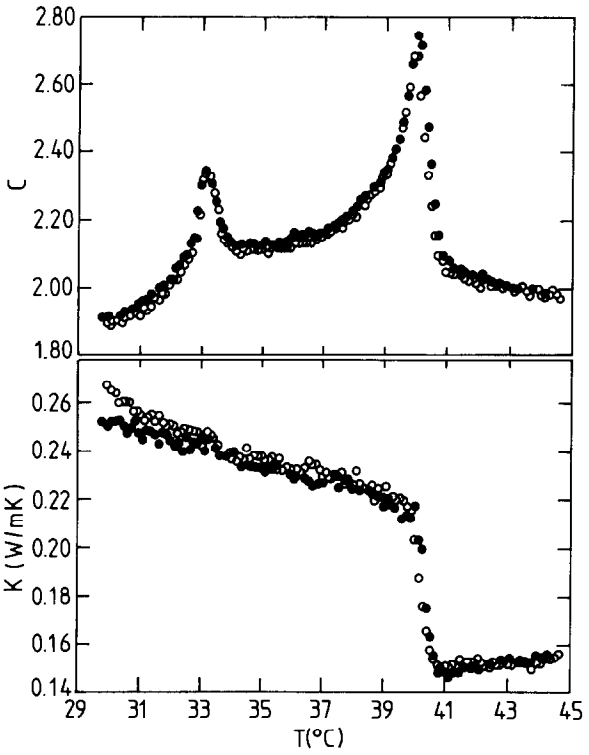


Fig. 8. Specific heat capacity and thermal conductivity as a function of temperature for a 8CB liquid crystal sample as determined photoacoustically. Solid dots are results without a magnetic field, and open circles are results for a magnetic field perpendicular to the sample surface.

Due to the strong homeotropic free surface alignment of the liquid crystalline molecules, it was not possible to obtain a homogeneous planar sample with a photoacoustic configuration, even with rather strong magnetic fields [38,40]. This problem can be overcome by using the photopyroelectric setup given in Fig. 3. By using this configuration one has the possibility to put the sample between two plates: at one side the pyroelectric transducer and on the other side the gold coated quartz piece that absorbs the incident modulated laser light and heats the sample. By applying a sufficiently thin polymeric coating on the surfaces of both the quartz piece and the pyroelectric

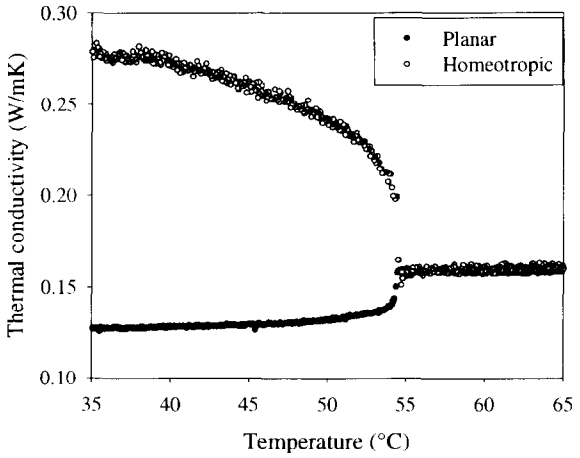


Fig. 9. Thermal conductivity of oriented (in the nematic phase) samples of the liquid crystal 6AB as determined with the photopyroelectric setup represented in Fig. 3.

transducer, planar as well as homeotropic alignment of the molecules can be imposed. Further enforcement of the molecules in the bulk of the samples (about 100 μm thick) can be realized by an additional magnetic field in the proper direction. Recently, we investigated photopyroelectrically planarly as well as homeotropically aligned samples of several compounds of the di-alkylazoxybenzene (nAB) homologous series [45]. Fig. 9 gives the thermal conductivity in the isotropic phase (high temperature) and in the nematic phase (low temperature) of 6AB. In the nematic phase a large difference between the $\kappa$ values for the homeotropic and planar samples is found. The corresponding specific heat capacity results (Fig. 10) are the same for both orientations (as expected for homogeneously aligned samples [38]) and show the usual critical anomaly at the nematic-to-isotropic transition near 55°C. Further details on the analysis of these results for 6AB and of other compounds of the nAB series will be given elsewhere [45].

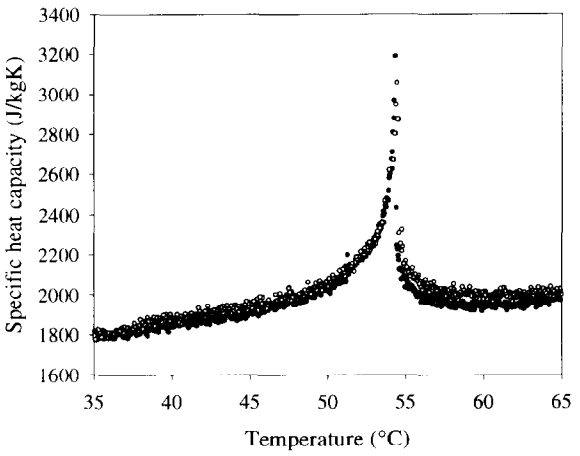


Fig. 10. Specific heat capacity data for the liquid crystal 6AB as obtained simultaneously with the thermal conductivity results given in Fig. 9.

## Acknowledgements

This work was financially supported by the Belgian National Science Fund (Grant N° G.0115.95). C.G. thanks the Onderzoeksraad (Research Council) of the Katholieke Universiteit Leuven for a post-doctoral fellowship.

## References

[1] A.G. Bell, Am. J. Sci, 20 (1880) 305.
[2] A.G. Bell, Phil. Mag., 11 (1881) 510.
[3] J. Tyndall, Proc. Roy. Soc. London, 31 (1881) 307.
[4] W.G. Röntgen, Phil. Mag., 11 (1881) 308.
[5] M.E. Mercadier, C.R. Acad. Sci. (Paris), 92 (1881) 409.
[6] W.H. Preece, Proc. Roy. Soc. London, 31 (1881) 506.
[7] M.L. Viengerov, Dokl. Akad. Nauk. SSSR, 19 (1938) 687.
[8] K.F. Luft, Z. Tech. Phys., 24 (1943) 97.
[9] M.L. Viengerov, Dokl. Akad. Nauk. SSSR, 46 (1945) 182.
[10] G. Gorelik, Dokl. Akad. Nauk. SSSR, 54 (1946) 779.
[11] P.V. Slobodskaya, Izv. Akad. Nauk. SSSR, Ser.Fiz., 12 (1948) 656.
[12] F.A. McDonald and G.C. Wetsel Jr., J. Appl. Phys., 49 (1978) 2313.
[13] F.A. McDonald, Am. J. Phys., 48 (1980) 41.
[14] A. Rosencwaig and A. Gersho, J. Appl. Phys., 47 (1976) 64.
[15] C. Glorieux, J. Fivez and J. Thoen, J. Appl. Phys., 73 (1993) 684.
[16] A. Rosencwaig, Photoacoustics and Photoacoustic Spectroscopy, John Wiley and Sons, New York, 1980.
[17] H.J. Coufal, R.K. Grygier, D.E. Horne and J.E. Fromm, J. Vac. Technol., A 5 (1987) 2875.
[18] A. Mandelis and M.R. Zver, J. Appl. Phys., 57 (1985) 4421.
[19] C. Christofides, Crit. Rev. Sol. State and Mat. Sci., 18 (1992) 113.
[20] E. Schoubs, H. Mondelaers and J. Thoen, J. Physique IV, C7 (1994) C7-257.
[21] E. Schoubs, Ph.D. thesis, Katholieke Universiteit Leuven, 1994.

[22] M. Marinelli, U. Zammit, F. Mercuri and R. Pizzoferrato, J. Appl. Phys., 72 (1992) 1096.
[23] C.W. Garland, Thermochimica Acta, 88 (1985) 127.
[24] I. Hatta, Y. Sasuga, R. Kato and A. Maesono, Rev. Sci. Instrum., 56 (1985) 1643.
[25] I. Hatta, Pure and Applied Chem., 64 (1992) 79.
[26] R. Geer, T. Stoebe, T. Pitchford and C.C. Huang, Rev. Sci, Instrum., 62 (1991) 415.
[27] C. Glorieux, J. Thoen, G. Bednarz, M.A. White and D.J.W. Geldart, Phys. Rev., B 52 (1995) 12770.
[28] G. Bednarz, D.J.W. Geldart and M.A. White, Phys. Rev., B 47 (1993) 14247.
[29] C. Glorieux, J. Caerels and J. Thoen, J. Appl. Phys., 80 (1996) 3412.
[30] C. Glorieux, Ph.D. thesis, Katholieke Universiteit Leuven, 1994.
[31] J. Thoen, in S. Martellucci and A.N. Chester (Eds.), Phase Transitions in Liquid Crystals, Plenum Press, New York, 1992, p. 155.
[32] C.W. Garland, in S. Martellucci and A.N. Chester (Eds.), Phase Transitions in Liquid Crystals, Plenum Press, New York, 1992, p. 175.
[33] J. Thoen, in S. Kumar (Ed.), Liquid Crystals in the Nineties and Beyond, World Scientific, Singapore, 1995, p. 19.
[34] J. Thoen, Int. J. Mod. Phys., B 9 (1995) 2157.
[35] T. Akahane, M. Kondok, K. Hashimoto and N. Nagakawa, Jpn. J. Appl. Phys., 26 (1987) L1000.
[36] M. Marinelli, U. Zammit, F. Scudieri and S. Martellucci, Nuovo Cimento, 9D (1987) 855.
[37] C. Glorieux, E. Schoubs and J. Thoen, Mater. Sci. Eng., A 122 (1989) 87.
[38] J. Thoen, C. Glorieux, E. Schoubs and W. Lauriks, Mol. Cryst. Liq. Cryst., 191 (1990) 29.
[39] U. Zammit, M. Marinelli, R. Pizzoferrato, F. Scudieri and S. Martellucci, Phys. Rev., A 41 (1990) 1153.
[40] J. Thoen, E. Schoubs, V. Fagard in O. Leroy and M.A. Breazeale (Eds.), Physical Acoustics: Fundamentals and Applications, Plenum Press, New York, 1992, p. 179.
[41] C. Glorieux, Z. Bozoki, J. Fivez and J. Thoen, J. Appl. Phys., 78 (1995) 3096.
[42] J. Thoen, H. Marijnissen and W. van Dael, Phys. Rev., A 26 (1992) 2886.
[43] M. Marinelli, F. Mercuri, U. Zammit and F. Scudieri, Phys. Rev., E 53 (1996) 701.
[44] F. Scudieri, M. Marinelli, F. Mercuri, U. Zammit, and S. Foglietta, Proc. 9th Int. Conf. on Photoacoustic and Photothermal Phenomena, Nanjing, China, June 27–30, 1996, Prog. Nat. Science (China) 6 (1996) S-262.
[45] J. Caerels, E. Schoubs and J. Thoen, to be published.